Pakhotin *et al. Earth, Planets and Space* (2022) 74:109
https://doi.org/10.1186/s40623-022-01668-5

Earth, Planets and Space

FULL PAPER Open Access

The swarm Langmuir probe ion drift, density and effective mass (SLIDEM) product

I. P. Pakhotin[1*], J. K. Burchill[1], M. Förster[2,3] and L. Lomidze[1,4]

Abstract

Current methods for estimating ion density on Swarm rely on the assumption of 100% O+ and no along-track ion velocity flows. These assumptions are routinely violated, particularly on the nightside and during high-latitude and polar cap traversals, compromising the accuracy of the measurements. The use of faceplate current data along with the Langmuir probe ion admittance measurements, and orbital-motion limited (OML) theory, make it possible to relax some of the assumptions inherent in current ESA Swarm density estimates. This further yields along-track ion drift and effective ion mass estimates. This paper describes the theoretical basis for estimating revised ion density, providing a new estimate for effective ion mass, as well as an alternative way of estimating along-track ion drift. The complete Swarm historical data set has been generated and validated using empirical models (International Reference Ionosphere, and an empirical electric field model), as well as ground-spacecraft conjunctions. Case studies and statistical results reveal clear geophysical signatures in the new product of light ions at low- and mid-latitudes and along-track ion drift at high latitudes, and their response to space weather.

Key points

- A new data product for Swarm along-track ion drift velocity, density and effective mass has been derived
- The addition of faceplate current to ion admittance enables a refinement to Swarm ion density
- The estimations have been validated against a variety of independent measurements and empirical models

Keywords: Plasma density, Ionospheric composition, Ionospheric convection, Langmuir probe, Ionosphere, Space weather

*Correspondence: pakhotin@ualberta.ca

[1] Department of Physics and Astronomy, University of Calgary, Calgary, AB, Canada
Full list of author information is available at the end of the article

Springer Open

© The Author(s) 2022. **Open Access** This article is licensed under a Creative Commons Attribution 4.0 International License, which permits use, sharing, adaptation, distribution and reproduction in any medium or format, as long as you give appropriate credit to the original author(s) and the source, provide a link to the Creative Commons licence, and indicate if changes were made. The images or other third party material in this article are included in the article's Creative Commons licence, unless indicated otherwise in a credit line to the material. If material is not included in the article's Creative Commons licence and your intended use is not permitted by statutory regulation or exceeds the permitted use, you will need to obtain permission directly from the copyright holder. To view a copy of this licence, visit http://creativecommons.org/licenses/by/4.0/.

Graphical Abstract

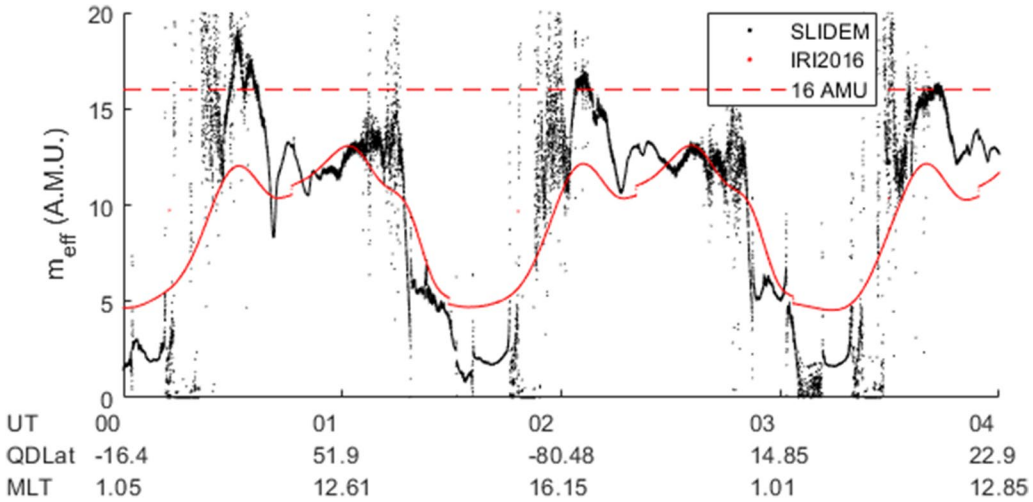

Introduction

Accurate measurements of key ionospheric parameters, such as density, ion species composition, and ion flows, are of crucial importance in studies of magnetosphere–ionosphere coupling (MIC) and determine the dynamics of magnetosphere–ionosphere–thermosphere energy transfer. In particular, the auroral zone is known to be a key interface where energy and momentum is transferred between the two systems at a range of spatio-temporal scales. As ion velocities are routinely used to estimate electric fields via $\mathbf{E} = -\mathbf{v} \times \mathbf{B}$ (e.g., Knudsen et al. 2017; Pakhotin et al. 2018), accurate measurements of these flows allow for better understanding of electromagnetic transverse disturbances, in the form of both Alfven waves and field-aligned currents (FACs), which provide the basis of the magnetosphere–ionosphere interface. While models such as the Weimer (2005) electric field empirical model, and ground radar observations such as SuperDARN (Greenwald et al. 1995) can estimate convection flows, they inherently focus on larger spatial and temporal scales. Meanwhile, recent works (e.g.,Codrescu et al. 1995; Rother et al. 2007; Pakhotin et al. 2018, 2020, 2021; Verkhoglyadova et al. 2017, 2018) demonstrate that small- and meso-scale disturbances can be responsible for a significant total portion of the energetics of MIC. These scales are inherently going to be missed by both large-scale empirical models and by ground radar-based measurements, and require in-situ observations by satellites, such as Swarm sampling at ≤ 1 Hz frequencies.

The primary method for measuring ion flows on Swarm is using the Thermal Ion Imager (TII) (Knudsen et al. 2017). Despite periods of degraded data quality arising from residual water vapour and spacecraft–plasma interactions, a robust cross-track ion velocity data set has been established (Lomidze et al. 2019, 2021; Koustov et al. 2019) and has been utilized in scientific studies including long-duration statistical Poynting flux studies (e.g., Pakhotin et al. 2021). Estimating the along-track component of ion drift is inherently more challenging, and to date a reliable along-track ion drift data set is unavailable (Knudsen et al. 2017; Burchill and Knudsen 2020). Clearly there is a need for reliable estimates of this component for the full 3D vector to be reconstructed.

The Swarm plasma instrumentation is complemented by a Langmuir probe. The plasma instrumentation also controls the electrical bias of the faceplate covering the TII and measures the current closing through it. The faceplate thus has a functionality similar to that of a planar Langmuir probe. This combination of spherical and planar Langmuir probes complements the standard methods for estimating plasma density and electron temperature estimates, which is exploited in this work. Further details are given in the "Data and Methodology" Section.

One aim of this paper is to detail an alternative method for measuring ion along-track flow component at high latitudes, utilizing orbital-motion limited (OML) theory (Mott-Smith and Langmuir 1926) and the faceplate current measurement, as well as Langmuir probe ion admittance. Since the ion velocity measurement is obtained using a different methodology, it is immune from some of the caveats associated with the classic TII measurement, and as such, forms a valuable addition to the Swarm data product family.

The low latitude ionosphere, meanwhile, is dominated by a range of density perturbations and changes associated with, for example, equatorial plasma bubbles (Woodman and La Hoz 1976), equatorial plasma fountains (e.g., Balan and Bailey, 1995), the Sq current system (e.g., Vasyliūnas 2012; Yamazaki and Maute 2017), Appleton anomaly (Appleton 1946), and others. Typically, these phenomena are not associated with strong drifts, but are heavily dependent on density and ionospheric composition. Studies of near-equatorial Alfven waves, in the form of field-line resonances, and interhemispheric Poynting flux transfer as, e.g., MSTIDs (Park et al. 2016), as well as space weather dynamics, such as ring current evolution (e.g., Ganushkina et al. 2015), also depend on accurate low-latitude estimations of density and ion composition. Ideally, the composition of individual ions would be measured directly by means, such as mass spectrometry. Swarm does not have such instruments on board, and in addition there are known sensitivity issues with mass spectrometers which may prevent them from observing accurate ion composition of cold or warm plasma. Instead, the swarm Langmuir probe ion density and effective mass (SLIDEM) methodology allows for the determination of an ion fraction, which is a parameter that is sensitive to the presence of light ions. As such, even small (< 5%) deviations from 100% O+ at low latitudes may be observed using this method.

Swarm ion densities are typically estimated from admittance using a simplified form of OML theory equations, where density is calculated directly from ion admittance signal via

$$N_i = \frac{d_s v_s m_s}{2e^2 \pi r_p^2} \tag{1}$$

where N_i is the ion density, d_s is the ion admittance (the response of the Langmuir probe current to changes in the bias voltage, $d_s = \frac{\partial I}{\partial V_b}$), v_s is the plasma speed in the ram direction, m_s is the effective (or reduced) ion mass, e is the elementary charge, and r_p is the spherical Langmuir probe radius. By sweeping the bias traditional LPs record the I–V curve, and d_s would be its derivative. The Swarm LPs normally estimate the current and derivative in three regions of the I–V curve, including a negative bias for the ion current. The bias is modulated with a sinusoidal "ripple" and d_s is recorded as a complex admittance. The ripple sinus frequency is low (typically 128 Hz), consequently the real part of the admittance is equivalent to the traditional derivative dI/dV, with a negligibly small imaginary part. For a full derivation of (1) please refer to Knudsen et al. (2017), in particular Eqs. (6) and (11) of that manuscript, also please note the voltage in that paper is in 'energy' units, i.e., the voltage is multiplied by the elementary charge constant.

In calculating the density in the above manner, typically two assumptions are made: first, that the effective ion mass is 16 atomic mass units (AMU), i.e., that the surrounding plasma is 100% singly charged oxygen ions. The second assumption is that the plasma ram speed v_s is equal to the satellite speed, ~ 7.6 km/sec on Swarm A; in other words, no along-track ion drifts are assumed. Especially on the nightside and at high F-region altitudes, significant amounts of lighter ions, e.g., H+, are present (e.g., Smirnov et al. 2021). In addition, strong ion drifts in both along- and cross-track directions are common in the auroral zone. Thus it is reasonable to expect that both of these assumptions are often violated, compromising the density estimates. Recent studies revealed that the Swarm LP ion densities are overall 20–35% lower compared to their independent measurements (Lomidze et al. 2018, 2021; Larson et al. 2021).

By introducing the faceplate current measurement, it is possible to refine the density estimation while relaxing the above assumptions, resulting in more accurate estimations of this parameter. In addition, this approach may also yield either the effective ion mass, or the along-track ion velocity, depending on the latitude. The remaining parameter must then be estimated.

The methodology we propose here uses the known lack of significant along-track ion drifts at low to middle magnetic latitudes and consequently assumes the along-track ion velocity in those regions to be zero (co-rotating velocity does not impact the along-track component). Then, effective ion mass and density may be derived, from which the fraction of light ions may be estimated. However, at high latitudes, we must estimate the effective ion mass from, e.g., an empirical model to derive along-track ion velocity. Since we no longer rely on the assumption of zero velocity, we expect more realistic ion density estimates. The three parameters obtained in this manner are validated against estimates from empirical models, primarily using the International Reference Ionosphere 2016 or IRI-2016 (Bilitza et al. 2017; Truhlik et al. 2015) for effective ion mass and density comparisons, and the Weimer (2005) electric field model for along-track ion drifts.

The rest of the paper is structured as follows. "Data and Methodology" Section presents the OML equations and Swarm measurement details, as well as outlining the empirical models. "Results" Section presents case studies and statistical examples of the SLIDEM products and validation data sets, while "Discussion" Section discusses the validity of the products. "Conclusions" Section summarises the paper.

Data and methodology

In this section, the theoretical basis for estimating along-track ion drift and effective ion mass from the Swarm measurements and an empirical high-altitude ion

composition model is introduced. Empirical models and incoherent scatter radar data used for data validation are described.

Swarm measurements and OML equations

The Swarm mission (Friis-Christensen et al. 2008) was launched in 2013 into a low-Earth polar orbit. In the main science phase, Swarm A and C fly side by side with a 1.4 degree cross-track separation at the equator and a varying along-track separation, typically ~ 10 s, at an altitude of ~ 450 km in the beginning of the main science phase. Meanwhile, Swarm B orbits ~ 60 km higher, with its local time typically different from that of Swarm A/C. The spacecraft are equipped with the 50 Hz Vector Field Magnetometer Merayo et al. (2008) as well as Thermal Ion Imagers to obtain ion velocity drifts at up to 16 Hz, a pair of Langmuir probes to obtain ion density and electron temperature estimates at 2 Hz, and a planar fixed-bias probe ("faceplate") for current measurements at 16 Hz (Knudsen et al. 2017).

The Langmuir probes operate > 99% of the time in what is known as the Harmonic Mode (Knudsen et al. 2017). This allows them to sample electric current and admittance parameters for three separate regions of the Volt–Ampere characteristics: "ion", "linear electron" and "retarded electron". For the purposes of this paper we use only the ion admittance, which, for a straightforward OML approximation, is given by (Knudsen et al. 2017)

$$d_i = \frac{\partial I}{\partial V_b} = \frac{2N_i e^2}{M_{eff} \nu_i} \pi r_p^2 \tag{2}$$

where d_i is the ion admittance, I is probe current, and V_b is the applied bias. As the right-most side of Eq. (2) indicates, the ion admittance is a function of ion density N_i, effective ion mass M_{eff}, and ion ram velocity v_i, as well as Langmuir probe radius r_p, and ion net charge, assumed to be the elementary charge e. The ESA Level 1b density estimate uses this equation, assuming a 100% O+ ionosphere ($M_{eff} = 16$ A.M.U.) and no along-track ion drifts such that $v_i =$ ~ 7.6 km/sec is the satellite speed.

Because the ion admittances of individual ion species sum in proportion to their relative concentrations, the effective ion mass in the above equation, in contrast to average mass, is equal to the reciprocal of the reciprocals of the constituent species:

$$\frac{1}{M_{eff}} = \frac{1}{N_i} \sum_{s=1}^{k} N_s \frac{1}{m_s} \tag{3}$$

where m_s is the mass of the sth ion species. It is also referred to as reduced mass. A feature of this parameter is that it is much more sensitive than average mass to small amounts of light ions. For example, even a 10% H+ fraction will reduce this value from 16 AMU to 6.4 AMU. It can be seen that in this scenario the density obtained under a 100% O+ assumption dramatically overestimates the true ion density. This effect is expected to be particularly strong on the nightside where higher concentrations of light ions can be present.

Similarly, the assumption of zero along-track ion drift can fail in the auroral zones where ion drifts of up to several km/s are not uncommon (e.g.,Lomidze et al. 2019; Archer et al. 2017). As such it can be seen that both of the assumptions used in calculating ion density are expected to be routinely violated.

One solution to this problem is to bring in current measurements from the Thermal Ion Imager (TII) faceplate. Neglecting the effects of plasma sheath, and assuming all ions have a single charge and flow at the same speed, the current collected by the frontal faceplate is

$$I_{FP} = -N_i e v_i A_{FP} \tag{4}$$

where A_{FP} is the faceplate area (804 cm^2). Equation (4) may be combined with Eq. (1) to obtain revised expressions for high-latitude ion density N_i

$$N_i = \sqrt{\frac{-d_i I_{FP} M_{eff}}{2e^3 A_{FP} \pi r_p^2}} \tag{5}$$

and along-track ion drift

$$v_i = v_{sat} - \sqrt{\frac{-2e\pi r_p^2 I_{FP}}{d_i A_{FP} M_{eff}}}. \tag{6}$$

The effective ion mass must still be assumed; for this study we use the IRI 2016 high-altitude ion composition model (Truhlik et al. 2015) to calculate an empirical effective ion mass based on four ion species (O+, N+, He+, and H+).

Similarly, at low-to-mid-latitudes the along-track ion drift may be neglected in comparison with the satellite speed, yielding

$$m_{eff} = \frac{-2e\pi r_p^2 I_{FP}}{d_i A_{FP} v_{sat}^2} \tag{7}$$

The faceplate bias is at times set to -1 V to optimize the TII science operations (Knudsen et al. 2017). However, this bias seems to not sufficiently repel electrons which then can contaminate the ion current. To obtain reliable ion density estimates the bias is set to the more negative − 3.5 V whenever the TII operations allow it (~ 10–70% of the time). SLIDEM product measurements are, therefore, available only when the faceplate voltage is set to − 3.5 V, amounting typically to several orbits per day until mid-2018. Swarm TII operations have required setting the faceplate voltage to − 1 V increasingly often in recent years, reducing the availability of SLIDEM products. A notable exception was that the faceplate was operated at

− 3.5 V almost continuously on Swarm C from mid-2019 to mid-2020. It should be noted that plasma sheath effects modify the effective areas of both the frontal faceplate and the Langmuir probe, such that they are not equal to their physical areas. For the faceplate, Particle-In-Cell simulations indicated that a correction factor for the effective area is required (Resendiz Lira et al. 2019):

$$\delta_{FP} = \frac{\alpha P \lambda_D}{A_{FP}} \left(1 - \frac{eV}{\frac{1}{2} M_{eff} v_{\perp}^2} - \beta \frac{eV}{kT_e} - \frac{\gamma}{eV} \frac{e^2}{4\pi \varepsilon_0 \lambda_D} \right) \quad (8)$$

where $\lambda_D = \left(\frac{\varepsilon_0 k T_e}{e^2 n} \right)^{1/2}$ is Debye length, k is the Boltzmann constant, T_e is electron temperature, V is potential (spacecraft floating potential plus faceplate bias), ε_0 is the permittivity of free space, $\alpha = 0.06929$, $\beta = 0.11552$, $\gamma = 66.0913 \times 10^6$ are fitting parameters. This δ_{FP} term may be applied in place of A_{FP}, e.g., $A_{eff} = A_{FP} * (1 + \delta_{FP})$.

Meanwhile, the Langmuir probe cross section is also modified by the plasma sheath effects; however, the geometry is more complex. As per (Resendiz Lira and Marchand 2021), since the probe is positioned near the negatively charged satellite body, lighter ions are preferentially deflected towards the satellite rather than towards the detector. As such, depending on ion composition, the effective area is generally smaller than the physical area. The equation, identical to Eq. 15 in Resendiz Lira and Marchand (2021), is as follows:

$$\delta_{LP} = \alpha \frac{\lambda_D}{r_p} \left(1 - \beta \frac{eV_f}{\frac{1}{2} M_{eff} v_d^2} - \gamma \frac{eV_f}{kT_e} \right) - \zeta V_f + \xi \quad (9)$$

where $\alpha = 7.996 \times 10\text{e}{-3}$, $\beta = 5.431$, $\gamma = 0.2191$, $\zeta = 5.915\text{e-}3$ / V and $\xi = -1.743\text{e}{-2}$. This correction factor is applied to probe area, $\pi r_p^{2*}(1\text{-}\delta_{LP})$. Thus the corrected form of Eq. (6) becomes:

$$v_i = v_{sat} - \sqrt{\frac{-2e(1-\delta_{LP})\pi r_p^2 I_{FP}}{d_i(1+\delta_{FP})A_{FP}M_{eff}}} \quad (10)$$

For the frontal faceplate, the effective area is generally larger than the physical area, while for the Langmuir probe, the effective cross-sectional area is generally smaller than the physical cross-sectional area. It can be seen then, that for both velocity and effective ion mass, the combined effects of the Langmuir probe and frontal faceplate plasma corrections generally act to make the numerator smaller and the denominator larger, i.e., to decrease both quantities. Meanwhile, the corrected density equation would be:

$$N_i = \sqrt{\frac{-d_i I_{FP} M_{eff}}{2e^3 A_{FP}(1+\delta_{FP})(1-\delta_{LP})\pi r_p^2}} \quad (11)$$

Provision has been made for post-processing the SLIDEM along-track ion drift to detrend slowly varying offsets across the polar regions. Mid-latitude drift, which can be several km/s in the raw estimates, are thereby zeroed at poleward quasi-dipole latitudes between 50 and 51 degrees. This approach is similar to the one used for the cross-track flow data set (Koustov et al. 2019; Lomidze et al. 2019; Burchill and Knudsen 2020).

Weimer 2005 empirical convection electric field model

The Weimer 2005 electric field model is an empirical electric potential and field model for the northern and southern hemisphere high-latitude regions, derived from DE-2 data between 1981 and 1983 (Weimer 2005). This model uses spherical harmonic fitting to obtain convection cell mapping as a function of solar wind parameters, such as IMF By, IMF Bz, solar wind speed, solar wind density, and AL Index. Recently, the Swarm TII cross-track ion velocity flows were validated against the Weimer (2005) model by Lomidze et al. (2019, 2021), who showed good statistical agreement between the two, similar large-scale median flow patterns, and examples of matching data for individual polar orbits. The methodology of Lomidze et al. (2019) is adapted to the present study to assess the validity of the SLIDEM along-track ion drift estimates. While the Weimer 2005 model is not generally expected to reproduce flows on a measurement-by-measurement basis, it is believed to be reliable when predicting gross features for relatively steady ionospheric conditions.

International reference ionosphere

The International Reference Ionosphere is a joint effort between COSPAR and URSI to obtain an international standard of key ionospheric parameters (Bilitza et al. 2017). The SLIDEM product includes empirical estimates of effective ion mass based on the latest high-altitude (>350 km) IRI ion composition model (Truhlik et al. 2015), which provides relative ion concentrations of O+, N+, He+, and H+. Although this model is not intended to reproduce Swarm measurements point-by-point, it serves as a solid basis for demonstrating expected trends in effective ion mass, and it is expected to be more reliable at high latitudes for the ion density and drift estimates than assuming pure O+. The IRI 2016 model is also used to obtain electron and ion temperatures and electron densities for product validation. The IRI is used here as a common reference to compare SLIDEM with respect to the existing L1b product, particularly to investigate the hypothesis that light ions on the nightside lead to significant errors in density when assuming pure O+. It is

noted that there is compelling evidence that IRI significantly overestimates topside ionospheric density (Bilitza and Xiong, 2021), particularly during low solar flux conditions. Thus, we expect both SLIDEM and L1b to systematically show lower ionospheric densities compared with IRI.

Incoherent scatter radar

A series of conjunctions between Swarm and the Jicamarca, Millstone Hill, Arecibo, RISR-C, RISR-N and Poker Flat radars were identified for statistical comparisons of the density measurements. The methodology is similar to that utilized in Lomidze et al. (2018), in particular plasma frequency was used in place of density, as high-density samples tend to affect overall characteristics of measurement discrepancies and estimates regression coefficients less severely in the frequency domain.

In addition, a set of seven overflights (conjunctions) by Swarm A of several incoherent scatter radar facilities (Evans, 1969) was identified to validate the measured faceplate current and ion admittance. The radar sites were chosen to cover equatorial (Jicamarca), middle (Millstone Hill) and high latitudes (EISCAT-Tromso). For each radar, one dayside and one nightside conjunction was identified. In addition, a second nightside conjunction was identified between Swarm A and Jicamarca, where the floating potential of Swarm A recorded an unusually low value (− 8.42 V), to investigate whether this would invalidate the SLIDEM methodology.

For each of the seven conjunctions, values for electron density and electron temperature have been obtained separately from the ground radar, from the Swarm satellite itself (using the Swarm SITE product (Lomidze et al. 2021)), and from IRI-2016. In addition, relative ion composition for H^+, He^+, N^+, and O^+ was obtained from IRI-2016. From these parameters the theoretical faceplate current and ion admittance have been estimated using the empirical correction models of Resendiz Lira et al. (2019) and Resendiz Lira and Marchand (2021), and the results are compared with the Swarm A measured faceplate current and high-gain probe ion admittance.

Results

This section presents statistical and time series data for the three primary outputs: ion density, effective ion mass, and the along-track component of ion drift. Intervals of data were chosen on the timescales of days to months to both demonstrate robustness of the results and to capture both seasonal and orbital variability. In particular, each Swarm orbit drifts on the timescale of months such that the ascending orbital track changes from the dayside, through dawn-dusk, to the nightside. For effective ion mass and density, the magnetic quasi-dipole (QD) argument of orbit parameter is used in place of latitude, where + 180 degrees is added to QD latitude values on the descending orbit track. This allows both the dayside and nightside tracks to be displayed on a single plot, showing differences in plasma density and effective ion mass day/night variation. The SLIDEM product generates effective ion mass estimates around the entire orbit, but measurements are flagged as valid only for quasi-dipole latitudes equatorward of ± 50 degrees. Ion drift is estimated only at quasi-dipole latitudes poleward of ± 50 degrees.

Density

A series of statistical conjunctions between Swarm and six incoherent scatter radar (ISR) ground stations were identified between 2014 and 2020 and analysed, following the methodology described in Lomidze et al. (2018, 2021). The results of the analysis are displayed in Fig. 1. The lines of best fit are calculated using orthogonal least squares. Swarm A, B and C are treated separately, with SLIDEM on the left and L1b on the right. Plasma frequency was used in place of density, following Lomidze et al. (2018). It can be seen that, for all cases, SLIDEM is slightly closer (by ~ 2–7%) to the theoretical one-to-one fit line (in cyan), though the difference is within the estimated errors.

An example of the time series of the density estimates obtained from SLIDEM (blue), from the existing ESA Level 1b product (red), and from the IRI model (black), is displayed in Fig. 2. Density variations with latitude are correctly captured by SLIDEM on the dayside and on the nightside. The dayside ionosphere exhibits higher densities, in line with expectations as this is the side exposed to EUV radiation. The nightside equatorial regions is where the difference between the two Swarm products is most pronounced. Since the nightside ionosphere may contain a higher fraction of light ions, its effective ion mass can be significantly different from the assumed 16 A.M.U. As such, SLIDEM is expected to exhibit an improved nightside ionosphere density estimation performance. It shows lower disagreements when compared with IRI, while the Level 1b product can be larger than IRI-2016 nightside densities by ~ 50%, as can be seen at 10:20 UT and at 11:50 UT in Fig. 2. This is in line with recent results suggesting that light ions lead to density over-estimations from Swarm Langmuir probe measurements (Xiong et al. 2022).

To examine longer periods, residuals are calculated by subtracting the densities obtained by SLIDEM from those obtained from IRI, as percentages of the IRI density values. The same is done for the Level 1b product to obtain residuals for that scenario. Both residuals are divided by IRI-2016 values to obtain relative percentage residuals,

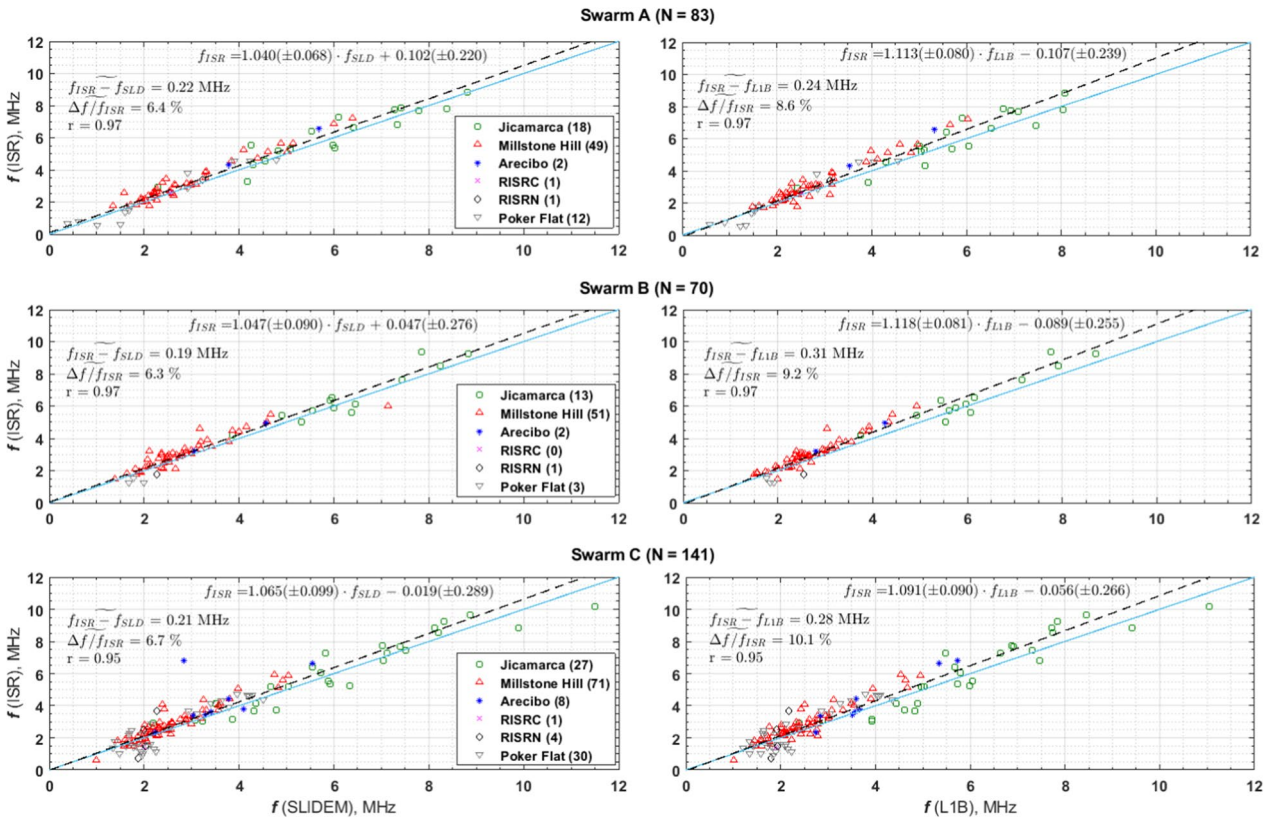

Fig. 1 ISR-Swarm conjunctions for Swarm A (top), Swarm B (middle) and Swarm C (bottom) panels. SLIDEM is on the left; L1b is on the right. The dashed black lines denote orthogonal-least-squares regression fits to the data, while the solid cyan line denotes a theoretical 'ideal' one-to-one correspondence. Both *x*- and *y*-axes are in units of MHz (plasma frequency) rather than density, following Lomidze et al. (2018) and references therein. The errors are given as standard errors at 95% confidence

which are then plotted in Fig. 3 as a function of time and magnetic quasi-dipole argument of orbit. The streaks of white background in the left-hand panel indicate unavailability of data. From Fig. 3, it can clearly be seen that the Level 1b product (right-hand panel) routinely returns higher nightside densities compared with IRI, as seen in Fig. 3b when the argument of orbit is between 0 and 50 deg. The improved agreement for the SLIDEM product (left-hand panel) is clear particularly with respect to overestimation, although both in-situ measurements show lower densities than IRI at systematic intervals, similar to Bilitza and Xiong (2021). For the time interval displayed in Fig. 3, the mean of the absolute of the residual between SLIDEM and IRI (Fig. 3a) is 43.9% (similar to the 42% bias for NeQuick topside option within IRI as detailed in Bilitza and Xiong, 2021), while that between the existing Level 1b density product and IRI (Fig. 3b) is 55.2%. Note, only those L1b-IRI2016 residual elements where data existed for SLIDEM-IRI2016 residuals were used in calculating the above values. The additional residual within L1b, beyond that expected for IRI/spacecraft comparisons, is believed to be due to the significant differences on the nightside due to effective ion mass deviating from 16 AMU. The SLIDEM methodology removes this assumption, yielding lower nightside residuals when compared with IRI-2016. A comparison between the SLIDEM and L1b densities (not shown) indicates the overall median difference of 17.3% but with noticeably larger L1b values on the nightside.

Effective ion mass

The effective ion mass time series for a representative time period are displayed in Fig. 4. It can be seen that, as Swarm traverses from dayside to nightside, the increasing fraction of light ions such as $H+$ decreases the effective ion mass to values much lower than 16 A.M.U. (red, dashed line). This is evidenced both by the IRI-2016 model (red) and SLIDEM observations (black). The SLIDEM effective ion mass estimates are not expected to be generally valid at higher latitudes as the spacecraft enters the auroral zone, since along-track ion velocity may no longer be neglected. Nevertheless, at lower latitudes

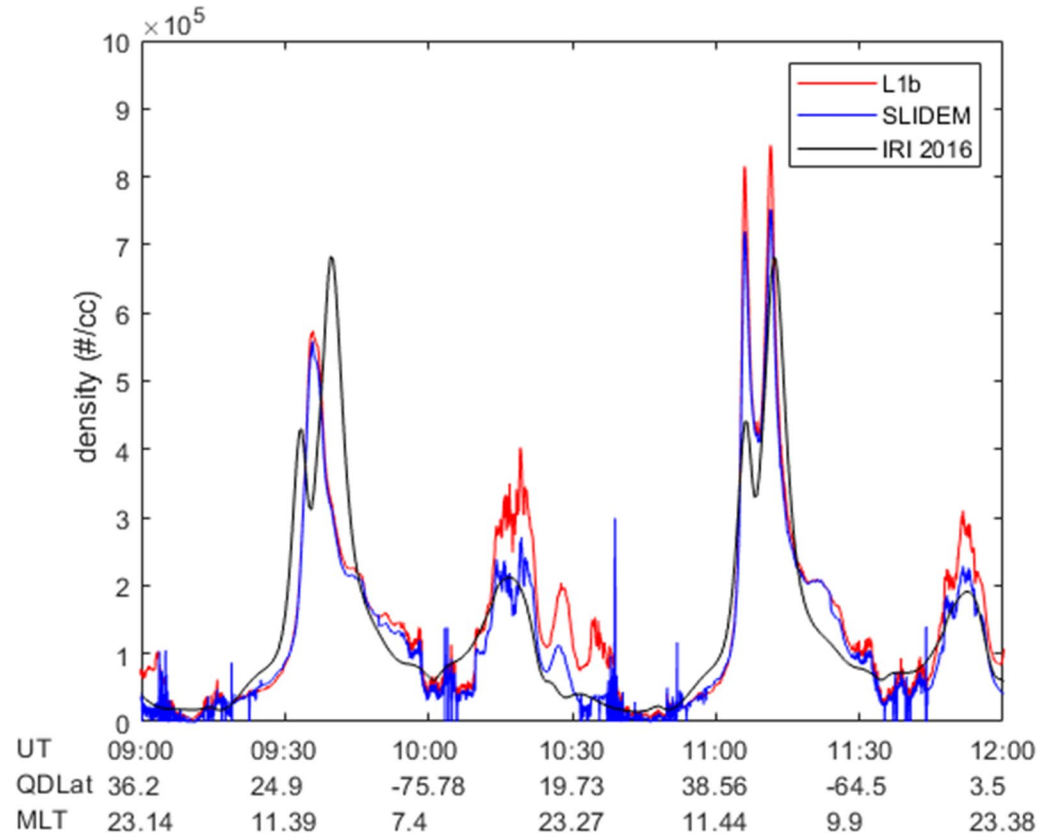

Fig. 2 Swarm A density estimations for 1 January 2018, using the SLIDEM methodology, the existing Level 1b estimate, and an independent measurement from IRI-2016

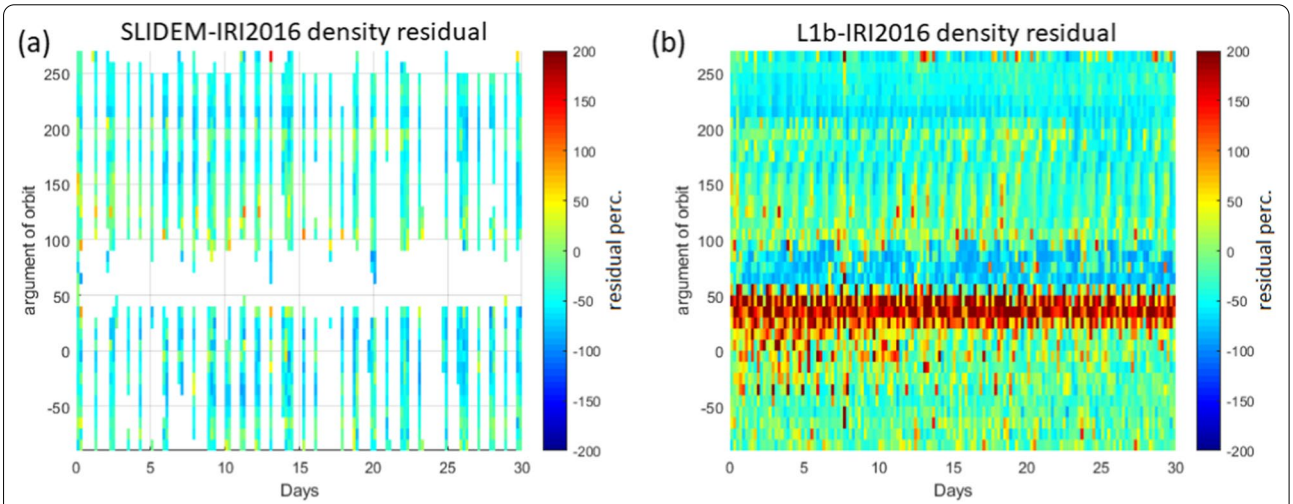

Fig. 3 Statistical analysis of the residual of density estimates between SLIDEM (IDM) and IRI-2016, as well as Level1b and IRI, for the time period 1–30 January 2018. Gaps in (a) denote periods of missing SLIDEM data coverage. Residuals are in units of percentage of the total density

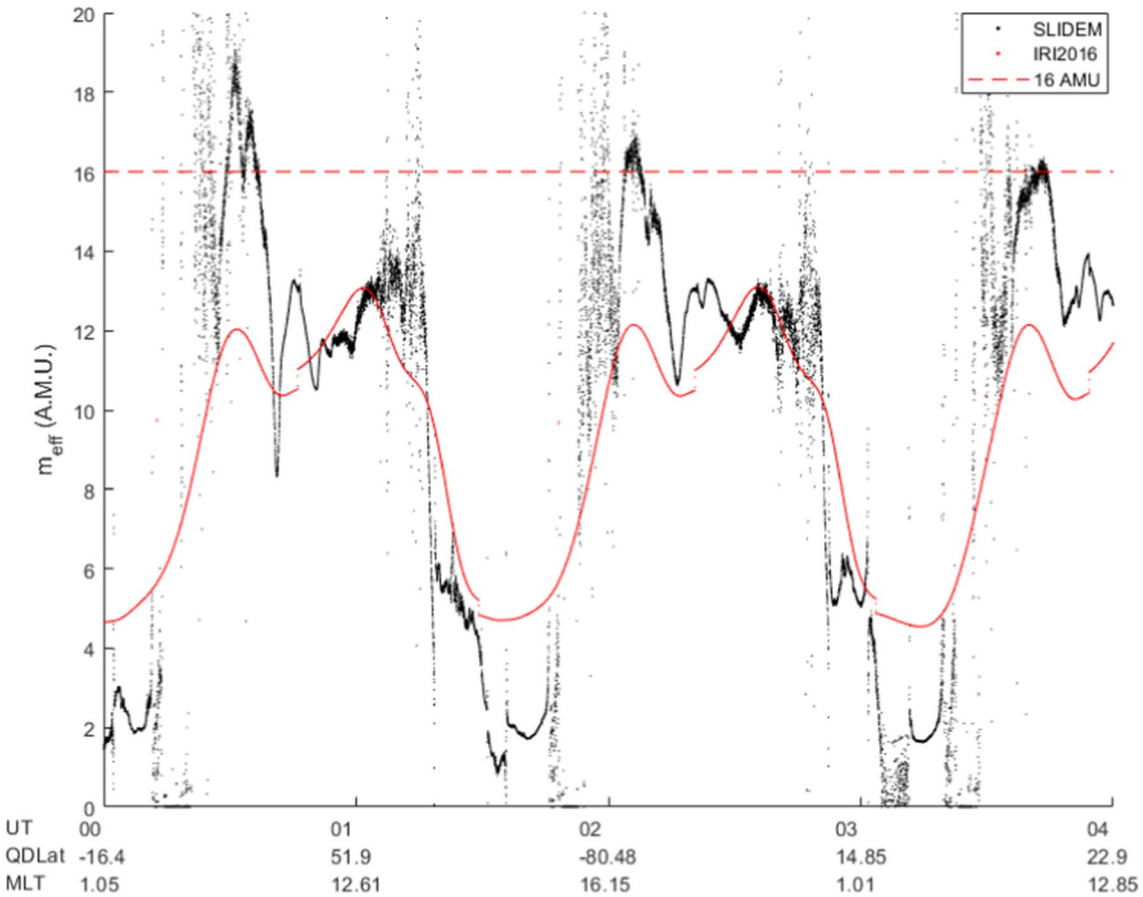

Fig. 4 Swarm A effective ion mass estimation using SLIDEM and IRI-2016 for a representative time period (1 May 2018). Data is shown for the entire orbit period, including times when significant along-track ion drifts are present

the agreement is good and small-scale features, as well as variations between consecutive orbits, are present in both the IRI-2016 and SLIDEM data. The SLIDEM estimate not unexpectedly shows more structure than the IRI model. All measurements are here plotted irrespective of quality flags to illustrate the range of variability and possible quality issues, such as effective ion mass occasionally falling below 1 AMU.

The effective ion mass estimates may be plotted against argument of orbit and time, as shown in Fig. 5 for one full year (2018). It can be seen that as the Swarm orbit drifts, the areas of low effective ion mass (typically found on the nightside) swap from the ascending track to the descending track. This is evidenced both in the IRI and in the SLIDEM product, and it can be seen that SLIDEM performs reasonably well at reproducing the effective ion mass at different local times.

Further analysis shows that SLIDEM is responsive to changes in space weather associated with variations in ion composition. Effective ion mass measurements for the 22 June 2015 storm (Tu et al. 2019) as obtained by SLIDEM (Fig. 6b, black) show significant changes in nightside effective ion mass on the timescale of hours, e.g., around day 22.4 in June 2015, suggestive of additional O+on the nightside (e.g., Kistler et al. 2016). These changes are captured by IRI-2016 (Fig. 6b, red) but as that model is parametrized by daily input parameters, the effective ion mass for IRI-2016 changes abruptly around the diurnal change line, which is not physically accurate. In this sense, SLIDEM provides superior estimates of effective ion mass than IRI-2016 during intense geomagnetic storms.

Ion velocity

In Fig. 7a plots are along-track ion drift estimates for auroral zone crossings on 28 Oct 2014. The direct output of the SLIDEM algorithm, obtained using Eq. (10), is shown in the light-gray points. Variability of order 1 km/s is evident, with respect to random errors (measurement resolution) of much less than 100 m/s. The systematic flow towards the satellite is interpreted as the measurement accuracy (~0.8 km/s). Detrending the resulting

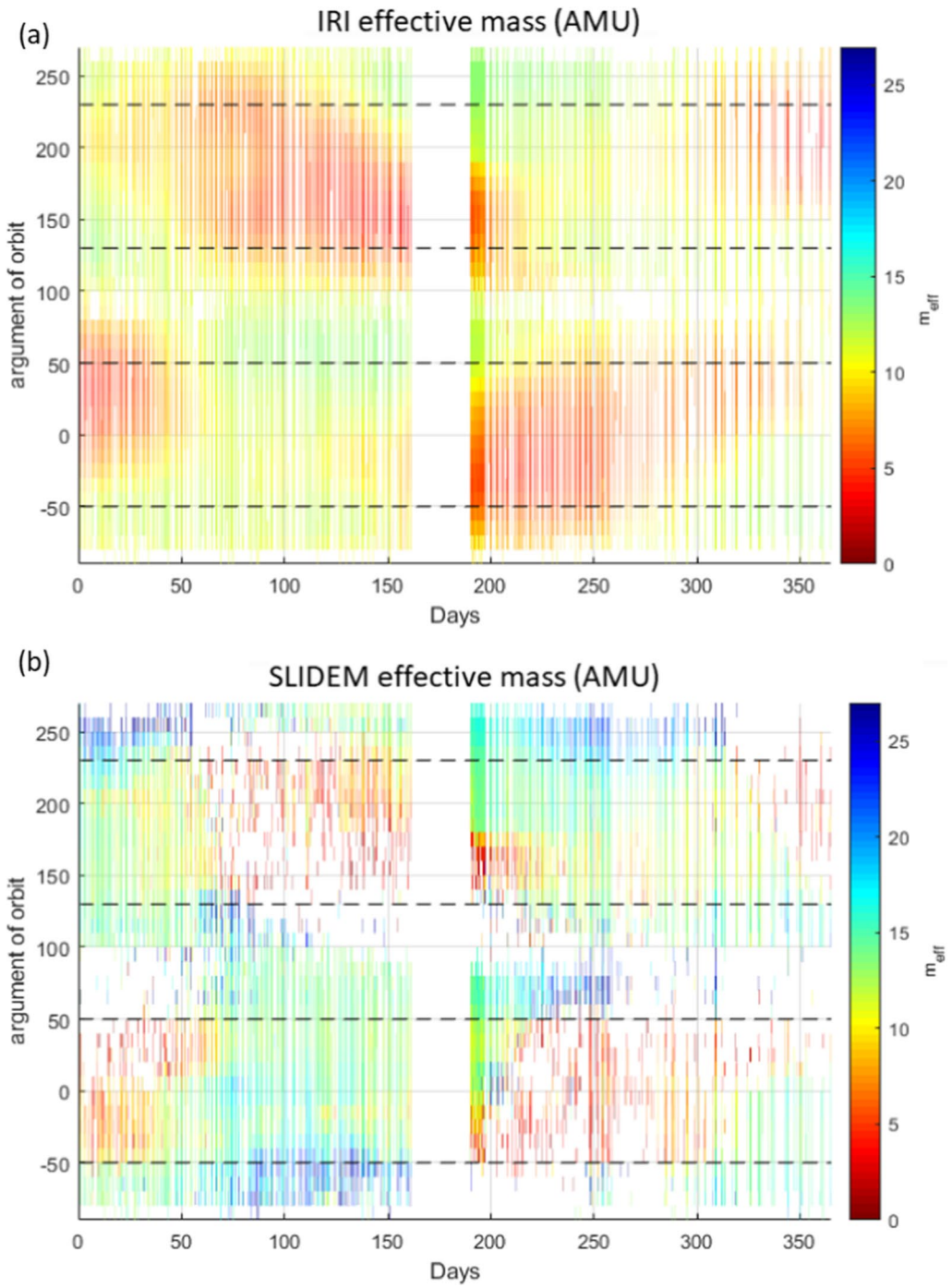

Fig. 5 Year-long plot of effective ion mass for Swarm A for the year 2018, for IRI-2016 **a** and SLIDEM (**b**). The colorbar is inverted, i.e., red colours denote periods of lower effective ion mass. The *y*-axis is quasi-dipole latitude. The dashed lines delineate the periods of validity, since significant along-track ion drifts are expected to be present at higher latitudes

drift, using the method applied to cross-track TII calibration (Burchill and Knudsen 2020), allows to capture the correct range of the drift during the auroral crossing, while ensuring it is around zero at lower latitude. The resulting detrended drift time series (black points) clearly show significant drift-related disturbances of geophysical origin at high latitudes, with drift settling down at mid-latitudes.

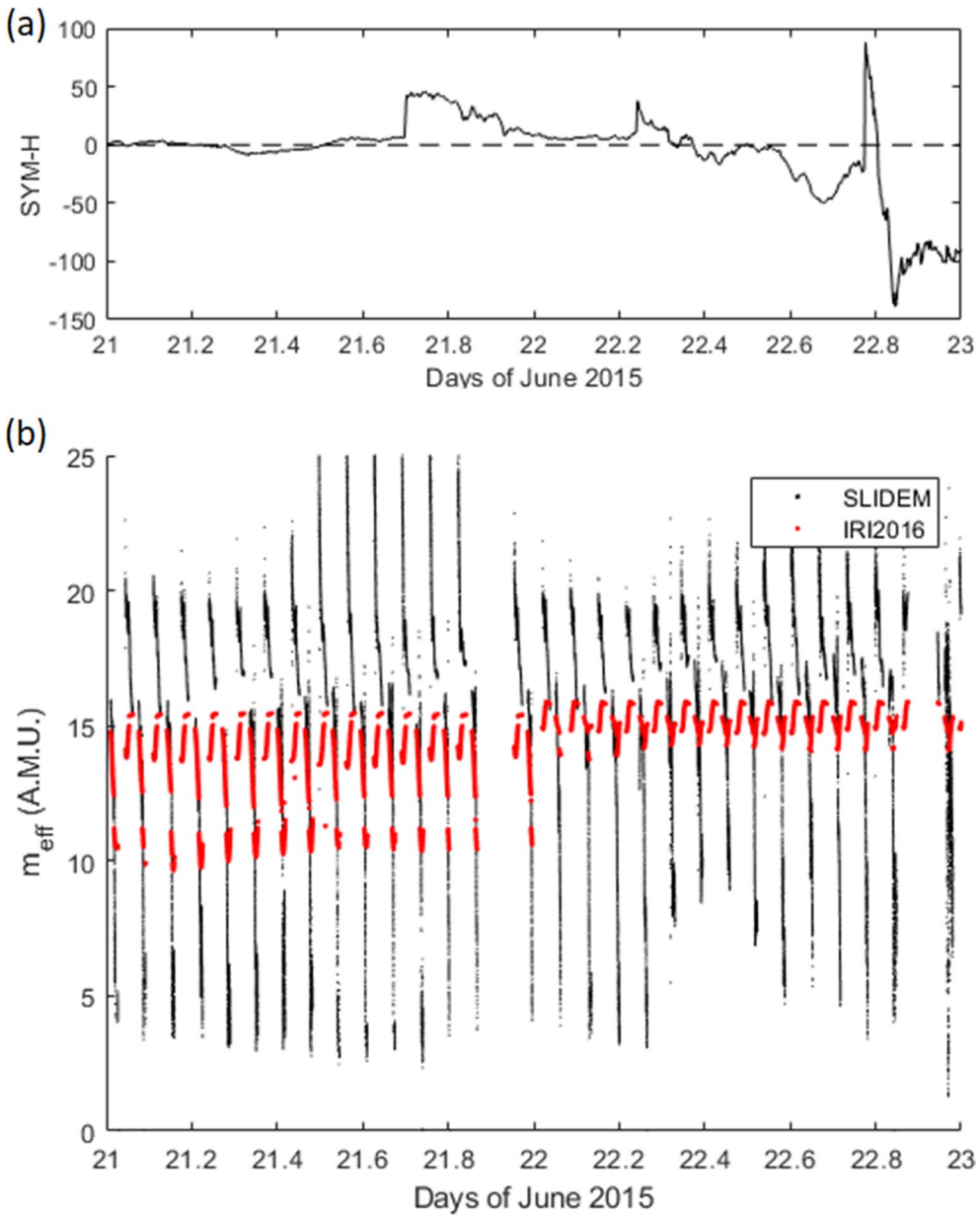

Fig. 6 Plot of the SYM-H **a** as well as Swarm A IRI-2016 and SLIDEM M_{eff} estimates for the time around the 22 June 2015 storm, denoting the change in effective ion mass during this active time period. In this plot, M_{eff} estimates outside of the validity range of this parameter (i.e., at high latitudes) are omitted both for SLIDEM and for IRI-2016

Figure 7b shows an example time series plot of an auroral zone crossing with such SLIDEM estimates of ion velocity, downsampled to 0.25 Hz (red). Output from the Weimer (2005) electric field model, obtained following to Lomidze et al. (2019), is plotted in blue. At large scales the data exhibits near perfect agreement with the model, correctly capturing drift dynamics including reversals at the right times. Smaller-scale signal is present on top of the large-scale convection, suggestive of large-magnitude, small-scale Alfven waves embedded within the large-scale FACs (e.g., Rother et al. 2007; Pakhotin et al. 2018, 2020).

To further evaluate the validity of ion drifts, following the same methodology as Lomidze et al. (2019), statistical maps of SLIDEM along-track drift data, obtained by calculating median components of drifts as a function

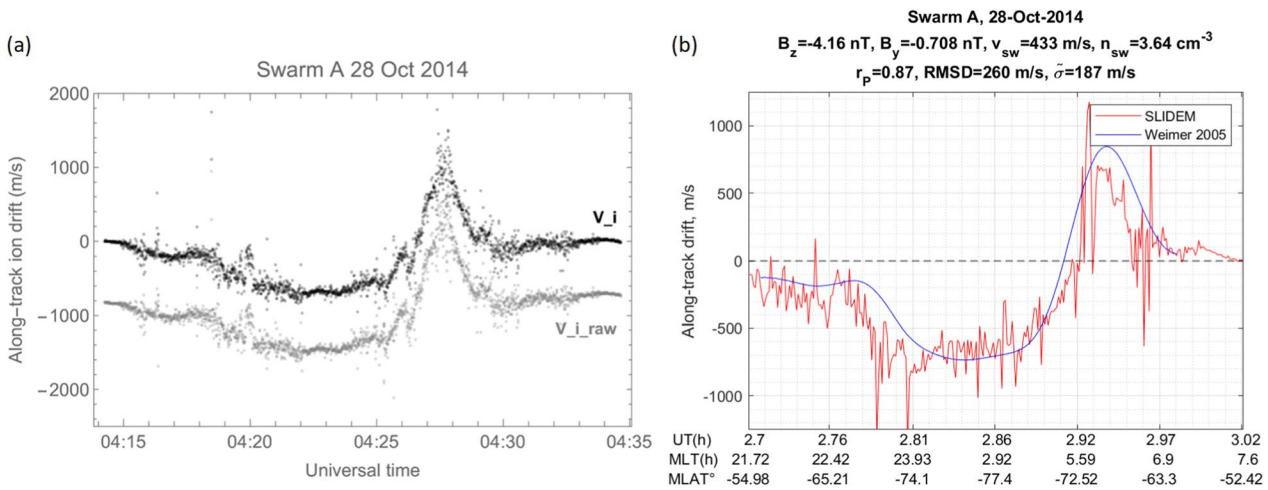

Fig. 7 for a representative auroral zone crossing, **a** shows along-track drift estimation using the SLIDEM methodology using various methods. The gray plot in **a** shows the along-track ion velocity estimate derived using Eq. (10), where effective ion mass has been estimated using IRI-2016. Meanwhile, the black plot shows the detrended version of the gray plot, to normalize it such that ion drift at low latitudes is around zero. **b** Shows a different auroral zone crossing on the same day, with the SLIDEM ion velocity output (red) alongside Weimer 2005 ion drift estimations (blue)

of magnetic latitude and local time, were created and compared with corresponding Weimer 2005 model drifts. Polar plots of the magnetic eastward projection of along-track drift are displayed in Fig. 8 for Swarm A in the southern hemisphere. The SLIDEM product captures some of the topology associated with the high-latitude ion convection, as well as its dependence on the direction of the IMF. For IMF $B_y > 0$ condition (left and middle panels of Fig. 8) both the SLIDEM and Weimer (2005) data show eastward (positive) flows around − 80° and westward (negative) flows around − 70° in the post-noon sector. For $B_y < 0$ conditions (right panel in Fig. 8) the overall agreement is also reasonably good poleward of ~ − 70°. Furthermore, the B_y-dependent asymmetry, i.e., change from predominantly westward to eastward flows poleward of 70° as B_y changes from positive to negative (left and middle panels vs right panel in Fig. 8) is evident from Weimer 2005 model and well reproduced by the SLIDEM data. The consistency, however, is generally poor for the dawn sector around − 70°, where Weimer 2005 shows eastward flows, while the SLIDEM shows only the reduced westward drifts. The ion convection typically becomes more intense when the IMF is southward as indicated by the Weimer model. The corresponding pattern seems to be largely missing from the SLIDEM data in Fig. 8; however, a clear pattern appears in the northward ion drift component (not shown). Part of the noted discrepancies are possibly due to remaining baseline/bias issues in the SLIDEM product. Others indicate certain limitations of the data and thus provide opportunity for their further refinement.

Incoherent scatter radar overflights

For the ground-spacecraft conjunctions, theoretical values for faceplate current and admittance were calculated using the SLIDEM methodology, using inputs from the radar measurements, from Swarm A, and from IRI-2016. They were then compared with actual observed current and admittance measurements. Figure 9 shows the faceplate current (a) and ion admittance (b) measurements from Swarm A vs theoretical values calculated from radar (R), Swarm SITE (S), and IRI (I) estimates of electron density and temperature. Colours indicated the radar overflown (JRO—Jicamarca; MH—Millstone Hill; ET—EISCAT Tromso) and the part of the orbit (day, night, dawn, or dusk, and whether the satellite was ascending or descending in latitude). Both faceplate current and ion admittance follow the expected linear trend yet exhibit a significant amount of scatter. The significant scatter in the faceplate currents arise predominantly from large differences in estimated electron density between the radar, Swarm, and IRI model. The Swarm faceplate measurements are generally explained best by the in-situ density (SITE).

A significant amount of scatter may be expected particularly in the ion admittance due to small variations in the concentration of light ions. To illustrate this, Fig. 10 shows the theoretical empirically adjusted ion admittance as a function of effective ion mass for the dayside ascending Jicamarca overflight using the radar density and temperature estimates. The point at upper right is the theoretical admittance for the Swarm A dayside ascending overflight of the Jicamarca incoherent scatter

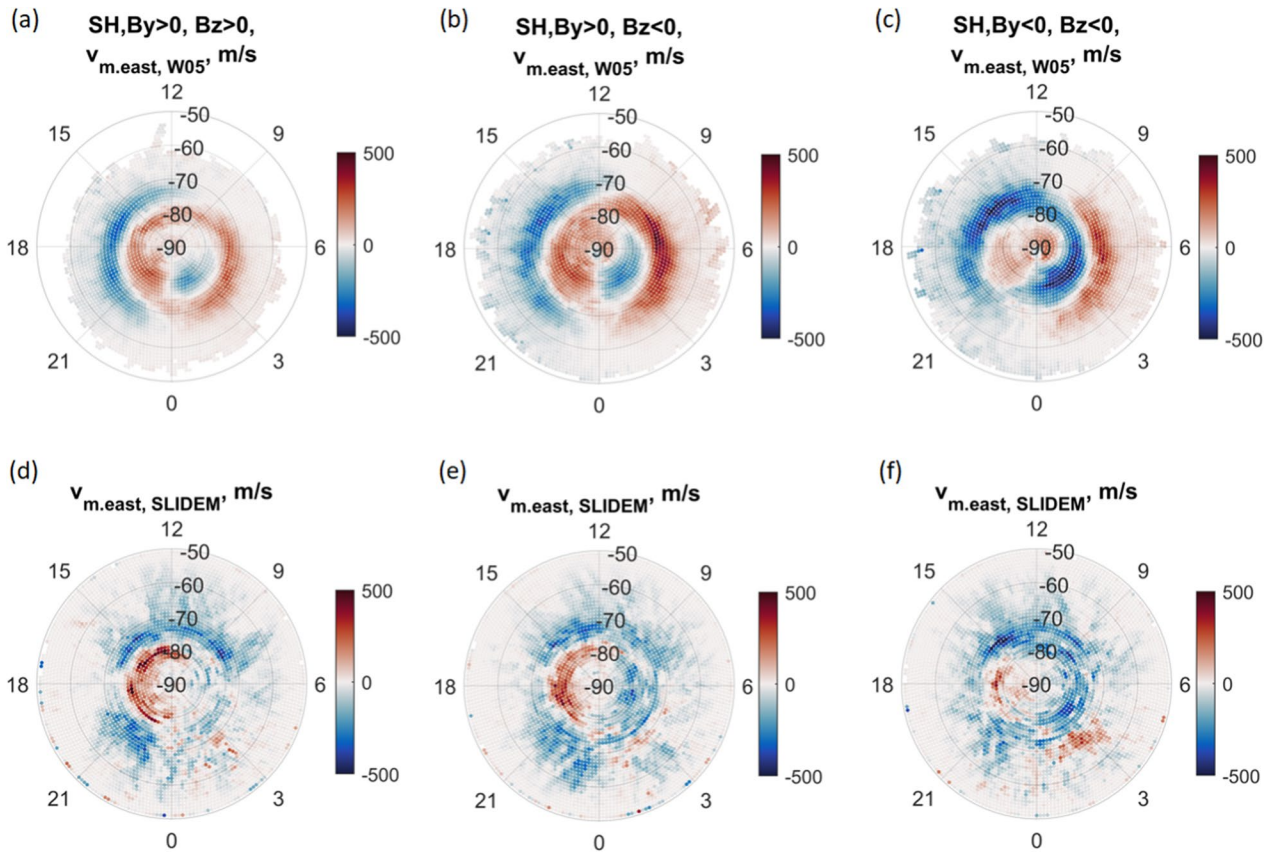

Fig. 8 Magnetic latitude-local time maps for Swarm A magnetic eastward ion drift components obtained from along-track data for different IMF conditions in the southern hemisphere. Northward IMF B_z, positive IMF B_y results are shown in **a** for Weimer (2005) and in **d** for SLIDEM. For southward IMF B_z and positive IMF B_y, Weimer 2005 is shown in **b** while SLIDEM is shown in (**e**). The case of southward IMF B_z and negative IMF By is shown in **c** for Weimer (2005) and in **f** for SLIDEM

radar facility, using the radar estimates for electron density and temperature and IRI estimates for ion composition. An increase to 3.5% H + with concomitant decrease to 94.9% O + (lower left point) decreases the expected ion admittance by almost 2 nA/V.

The spacecraft floating potential—which enters into several of the SLIDEM equations—is obtained from the Langmuir probes, as an average between the low-gain and high-gain probe. Figure 11 shows one day of data records (~ 16 orbits) of the floating potential differences between the two Langmuir probes as a function of QD latitude (blue curve). The two potentials usually disagree, sometimes by more than 1.5 V, a value much larger than the potential difference associated with e.m.f. from motion of the satellite through the geomagnetic field (red curve). The observations suggest the presence of strong electric fields in the vicinity of the instruments, or an issue with the calibration of the potential estimates, as well as the fact the two probes are made of different materials. The SLIDEM products are flagged for cases when the two probe estimates for floating potential differ by more than 0.3 V.

Discussion

The SLIDEM methodology aims to estimate three parameters using Swarm data:

- density
- effective ion mass
- along-track ion drift

In the process it also estimates the plasma sheath effects of the faceplate and Langmuir probe and the local Debye length, but these parameters are not investigated in this paper. For the three primary parameters of interest, the SLIDEM estimates are corroborated by empirical models and by space-ground conjugate measurements.

The primary advantage of density estimations using SLIDEM over existing Swarm L1b LP data is its ability to take into account the changes in ion composition in the

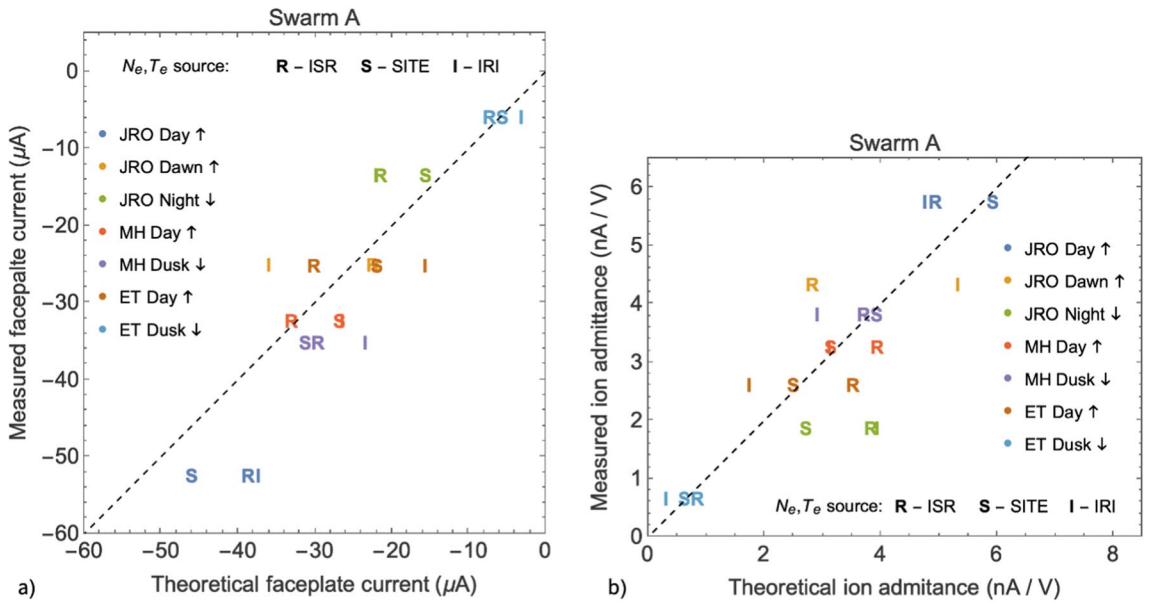

Fig. 9 Incoherent scatter radar facility validation. **a** Measured faceplate current vs theoretical current for each radar facility and for each of three estimates used for electron density and temperature. Ion composition was estimated using the IRI in all cases. **b** Measured vs theoretical ion admittance. Theoretical values include adjustments based on PIC simulations from Resendiz Lira et al. (2019) and Resendiz Lira and Marchand (2021)

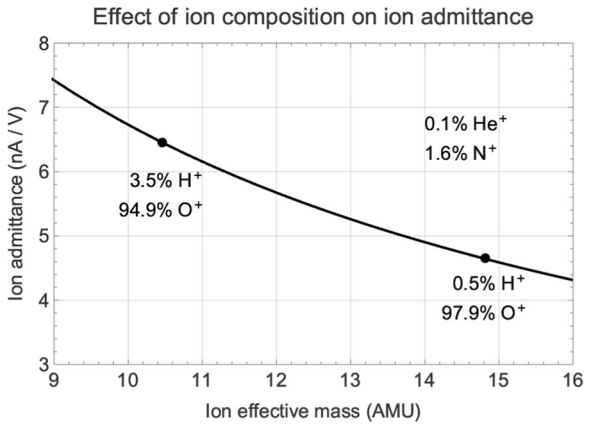

Fig. 10 Illustration of the large sensitivity of ion admittance to small variations in light ion composition. The point at lower right is the theoretical admittance for the Swarm A dayside ascending overflight of the Jicamarca incoherent scatter radar facility, using the radar estimates for electron density and temperature and IRI estimates for ion composition. An increase to 3.5% H + with concomitant decrease to 94.9% O + (upper left point) decreases the ion admittance by almost 2 nA/V

topside and removal of non-zero ion drift assumption at high latitudes. Our statistical analysis of density data yields better agreement with conjugate ISR observations (Fig. 1), with IRI-2016 (Figs. 2, 3), particularly on the nightside where light ions significantly change effective ion mass from the generally assumed 16 AMU. Similar to Bilitza and Xiong (2021) who showed—42% percentage deviation compared to other measurements, our results also show that the IRI overestimates densities in the topside ionosphere. Overall difference between the two Swarm products is smaller than that with IRI, however, assuming IRI better captures density variation related to the light ions, the smaller difference between the SLIDEM and IRI at night could indicate an advantage of the new data product.

Our results showed the SLIDEM values tend to be lower than those by Swarm LP on the nightside. Previous analysis of Swarm LP data (Lomidze et al. 2018, 2021; Larson et al. 2021), however, demonstrated that overall the Swarm data are 20–35% lower than those by other independent measurements. In those studies, coincident data from ISRs, ionosondes, and radio occultation were used, and all latitudes and local times were covered. The analysis of Swarm LP data at lower and middle latitudes during nighttime was part of the Lomidze et al. (2018) study who found ~ 4–12% lower Swarm densities (equivalent to 2–6% lower plasma frequencies) than those by the COSMIC radio occultation, thus the difference was smaller (less underestimation) than the overall trend. In addition, note that the period considered in that study (December 2013–June 2016) is characterized by a higher solar activity than January 2018 (considered for SLIDEM). The composition of light ions, furthermore, is known to be more significant at a given altitude in the topside for lower solar activity

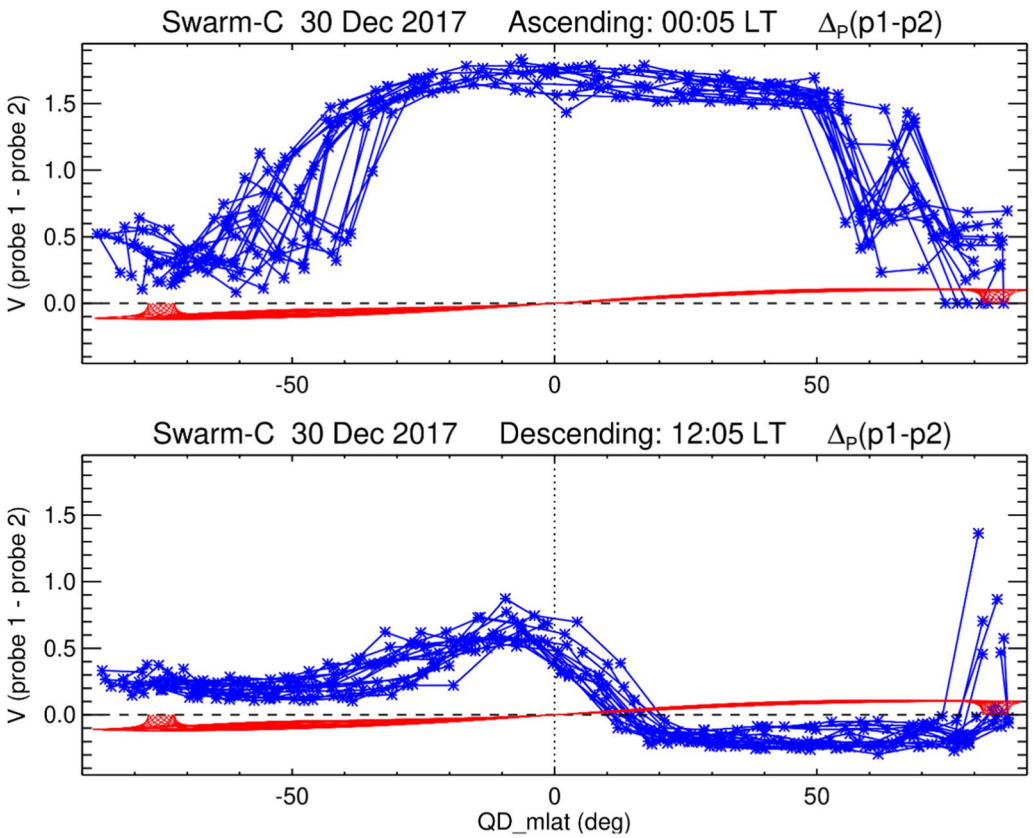

Fig. 11 Example of the difference of floating potential estimates between Langmuir probes 1 and 2 (blue) as a function of QD_Mlat, for nightside (ascending, top) and dayside orbits (descending, bottom). The red plot shows the theoretical inter-probe potential variation which may be expected as a result of electro-magnetic forces created by the spacecraft's motion

conditions at night. To better evaluate the performance of SLIDEM density, and understand how the low latitude, nighttime Swarm LP density accuracy varies compared to independent measurements as solar activity changes from high to low, it is important to extend the corresponding analyses to the entire Swarm mission in a future study.

For effective ion mass estimations, SLIDEM estimations correctly capture M_{eff} variations both as a result of orbital dynamics (Figs. 4, 5) and space weather (Fig. 6). The disagreement on the timing of the change in M_{eff} (Fig. 6) may likely be due to IRI-2016 not capturing the time-delayed chain of events which occur during a geomagnetic storm. Indeed, the model outputs instant values when initialized with a set of parameters. Meanwhile, a real magnetosphere has memory and information about what has happened in the past is necessary to correctly predict future behavior during rapidly changing geomagnetic conditions.

For along-track ion velocity estimation, (Fig. 7b), the employed scheme is capable of producing realistic ion velocity drifts which can be in good agreement with Weimer (2005) model estimates, capturing both the correct magnitudes as well as the large-scale structure. Smaller scale structures superimposed on the large-scale drifts is likely indicative of large-magnitude Alfven waves.

Climatology obtained using the SLIDEM drifts are capable of reproducing some of the main features of the high-latitude convection, in agreement with Weimer 2005. In particular, the westward drifts in the post-noon equatorward sector and the eastward drifts in the poleward noon sector, as well as the IMF B_y-dependent asymmetry and IMF B_z-dependent flow enhancements (for the northward drifts). Certain features, e.g., the eastward drifts in the equatorward morning sector and enhanced zonal drifts with southward IMF are not well-reproduced, and further analysis is needed. Overall, comparison results also imply the general level of accuracy of the ion drift attained, being of the order of several hundred m/s. Furthermore, the fact that the SLIDEM drifts are often of very small in magnitude equatorward of -60° is an indication of the effectiveness of the post-processing linear detrending. In general, the product would benefit

from further refinement to remove sources of uncertainty and investigate the effects of Langmuir probe plasma sheath effects more rigorously. Nevertheless, it is capable of producing reasonable agreement with independent model estimates and it may be possible to use SLIDEM along-track estimates to improve the quality of the TII along-track ion velocity estimations which currently suffer from known issues (Knudsen et al. 2017; Koustov et al. 2019).

A brief discussion of potential sources of uncertainty will follow. These present potential error sources which may be responsible for disagreement between SLIDEM products and independent estimates, particularly with along-track ion drift estimations.

Photoelectron effects refer to those electrons emitted as a result of solar irradiation of the satellite. Resendiz Lira et al. (2019) argue that these may be safely neglected on the nightside, and in areas of high density where collected ion currents exceed those from photoelectron emission. As a result, they do not appear in the faceplate nor the Langmuir probe effective area correction terms.

The geomagnetic field may be positioned in such a way that the Swarm body shields the Langmuir probe from incoming field-aligned electrons, whose small gyroradii mean they impact the satellite before the probe. If true, this effect should be observed on one hemisphere but not on the other, since the magnetic field will be 'disconnected' from the Langmuir probe on one side of the equator and 'connected' on the other from the magnetosphere side. There is some evidence of a small interhemispheric change in effective ion mass estimates (see, e.g., Fig. 4) which may be due to this effect, and it is worth exploring further. Nevertheless, it is not believed to be large enough to account for significant differences between simulated and measured admittance values. It should be noted that SLIDEM utilizes the ion admittance measurements (negative probe bias), and thus the admittance is not expected to be directly impacted by aforementioned electron dynamics.

Finally, the aforementioned ambiguities in spacecraft floating potential estimates, which often vary between the two probes, present a further potential error source, since this parameter enters into Eqs. (8) and (9) and thus affects the extent of the plasma sheath effects.

Conclusions

A new plasma density, effective ion mass and along-track ion velocity product has been developed, following OML methodology and relaxing the assumptions present in the existing Level 1b Swarm density estimation method. The new density data product has been validated through comparison with empirical models. A significant finding is that for the month-long period analyzed, the revised ion density estimate has consistently lower residuals with respect to IRI ion density, particularly on the nightside, when compared with the Level 1b methodology, due to improved estimation of the effective ion mass which deviates significantly from 16 AMU when light ions are present. Likewise, ground-satellite conjugate observations for the duration of the mission, using Swarm A, B and C, demonstrate that SLIDEM density estimations result in improved agreement with ground ISR density measurements when compared with the existing Level1b product. The effective ion mass estimations have also been compared with IRI and have been found to exhibit good agreement in longer, year-long comparison, reproducing changes in effective ion mass associated with space weather as well as due to Swarm orbital drift.

For along-track ion velocity, the data product was compared with the Weimer 2005 electric field model. Cases with good agreement were found for individual passes, while statistical analysis following Lomidze et al. (2019) demonstrated reasonable agreement reproducing some major features of global ion convection related to latitude, local time, and IMF variation. It is found that detrending the flows following the method used for TII cross-track ion velocities (Burchill and Knudsen 2020) is required. The future improvements in the data quality are needed to address some of the caveats that were found from the analysis.

A historical data set, PREL 0101, has been generated covering the same interval as the Swarm EXTD_LP_FP data set (2 October 2014 through 18 October 2021). The final product is anticipated to become available as one of the Swarm data products distributed via ESA EO PDGS. The link would be under "https://earth.esa.int/eogateway/missions/swarm/data". Currently it is available through FTP at "swarm-diss.eo.esa.int" in the "Advanced" folder. Data quality flagging is at an early stage of development; users are encouraged to read the SLIDEM Product Description Document (Pakhotin and Burchill 2021). It is anticipated that this data set will facilitate new scientific investigations in ionospheric physics and space weather as well as investigations into the Swarm TII ion drift and LP ion density data quality.

Appendix

Table of conjunction times between Swarm A and ground stations for data shown in Fig. 9. Data from Fig. 1 are for conjunctions selected from Lomidze et al. (2021).

Conjunction	Time (UT)
Swarm-A/Jicamarca (dayside)	2017-09-07 15:18
Swarm-A/Jicamarca (nightside)	2019-03-25 00:25
Swarm-A/Jicamarca (nightside)	2015-05-28 06:38
Swarm-A/Millstone Hill (dayside)	2015-04-10 22:33
Swarm-A/Millstone Hill (nightside)	2015-07-16 01:21
Swarm-A/EISCAT-Tromso (dayside)	2015-07-08 08:50
Swarm-A/EISCAT-Tromso (nightside)	2016-01-07 03:33

Acknowledgements
Prof. Richard Marchand (University of Alberta) provided feedback on a draft of this paper. The authors acknowledge helpful feedback from two anonymous referees.

Author contributions
JB and MF created and developed the concept including the mathematical foundations of the methodology, and performed preliminary analysis using Swarm and IRI-2016 data. IPP was mainly responsible with performing the analysis to quality SLIDEM data against IRI-2016, curating the conjunction list, and writing the manuscript. LL performed analysis of SLIDEM along-track ion drift estimates and operated the Weimer 2005 model to create the statistical and case study comparisons between the empirical model and the observations. All authors read and approved the final manuscript.

Funding
IPP was supported by the European Space Agency Swarm DISC SLIDEM contract. JKB was supported by funding from the Canadian Space Agency.

Availability of data and materials
Swarm data are available from ESA at http://swarm-diss.eo.esa.int. The IDL software for the Weimer 2005 model is available in the Zenodo repository (at http://doi.org/10.5281/zenodo.2530324). Millstone Hill, Jicamarca, and EISCAT-Tromso incoherent scatter radar data were obtained from the Madrigal database at http://www.openmadrigal.org/.

Declarations

Competing interests
The authors declare that they have no competing interests.

Author details
[1]Department of Physics and Astronomy, University of Calgary, Calgary, AB, Canada. [2]German Research Centre for Geosciences, Helmholtz Centre Potsdam, Potsdam, Germany. [3]Max Planck Institute for Solar System Research, 37077 Göttingen, Germany. [4]E. Kharadze Georgian National Astrophysical Observatory, Abastumani, Georgia.

Received: 4 February 2022 Accepted: 24 June 2022
Published online: 12 July 2022

References

Appleton E (1946) Two anomalies in the ionosphere. Nature 157:691. https://doi.org/10.1038/157691a0
Archer WE, Knudsen DJ, Burchill JK, Jackel B, Donovan E, Connors M et al (2017) Birkeland current boundary flows. J Geophys Res Space Phys 122:4617–4627. https://doi.org/10.1002/2016JA023789
Balan N, Bailey GJ (1995) Equatorial plasma fountain and its effects: possibility of an additional layer. J Geophys Res 100:21421–21432. https://doi.org/10.1029/95JA01555
Bilitza D, Xiong C (2021) A solar activity correction term for the IRI topside electron density model. Adv Space Res 68:2124–2137. https://doi.org/10.1016/j.asr.2020.11.012
Bilitza D, Altadill D, Truhlik V, Shubin V, Galkin I, Reinisch B, Huang X (2017) International Reference Ionosphere 2016: from ionospheric climate to real-time weather predictions. Space Weather 15:418–429. https://doi.org/10.1002/2016SW001593
Burchill J, Knudsen DJ (2020) EFI TII Cross-Track Flow Data Release Notes, Swarm Data, Innovation, and Science Cluster (Technical Report). Report No. SW-RN-UoC-GS-004, Rev. 5 (European Space Agency, 2020)
Codrescu MV, Fuller-Rowell TJ, Foster JC (1995) On the importance of E-field variability for Joule heating in the high-latitude thermosphere. Geophys Res Lett 22(17):2393–2396
Evans JV (1969) Theory and practice of ionosphere study by Thomson scatter radar. Proc IEEE 57(4):496–530. https://doi.org/10.1109/PROC.1969.7005
Friis-Christensen E, Luhr H, Knudsen D, Haagmans R (2008) Swarm—an Earth observation mission investigating geospace. Adv Space Res 41(1):210–216. https://doi.org/10.1016/j.asr.2006.10.008
Ganushkina NY, Liemohn MW, Dubyagin S, Daglis IA, Dandouras I, De Zeeuw DL, Ebihara Y, Ilie R, Katus R, Kubyshkina M, Milan SE, Ohtani S, Ostgaard N, Reistad JP, Tenfjord P, Toffoletto F, Zaharia S, Amariutei O (2015) Defining and resolving current systems in geospace. Ann Geophys 33:1369–1402. https://doi.org/10.5194/angeo-33-1369-2015
Greenwald RA, Baker KB, Dudeney JR, Pinnock M, Jones TB, Thomas EC, Villain J-P, Cerisier J-C, Senior C, Hanuise C, Hunsucker RD, Sofko G, Koehler J, Nielsen E, Pellinen R, Walker ADM, Sato N, Yamagishi H (1995) DARN/SuperDARN: a global view of the dynamics of high-latitude convection. Space Sci Rev 71:761–796
Kistler LM et al (2016) The source of O+ in the storm time ring current. J Geophys Res Space Phys 121:5333–5349. https://doi.org/10.1002/2015JA022204
Knudsen DJ, Burchill JK, Buchert SC, Eriksson AI, Gill R, Wahlund JE et al (2017) Thermal ion imagers and Langmuir probes in the Swarm electric field instruments. J Geophys Res Space Phys 122:2655–2673. https://doi.org/10.1002/2016JA022571
Koustov AV et al (2019) A comparison of cross-track ion drift measured by the Swarm satellites and plasma convection velocity measured by SuperDARN. J Geophys Res Space Phys 124:4710–4724
Larson B, Koustov AV, Kouznetsov AF, Lomidze L, Gillies RG, Reimer AS (2021) A comparison of the topside electron density measured by the Swarm satellites and incoherent scatter radars over Resolute Bay, Canada. Radio Sci. https://doi.org/10.1029/2021RS007326
Lomidze L, Knudsen DJ, Burchill J, Kouznetsov A, Buchert SC (2018) Calibration and validation of Swarm plasma densities and electron temperatures using ground-based radars and satellite radio occultation measurements. Radio Sci 53:15–36. https://doi.org/10.1002/2017RS006415
Lomidze L, Burchill JK, Knudsen DJ, Kouznetsov A, Weimer DR (2019) Validity study of the Swarm horizontal cross-track ion drift velocities in the high-latitude ionosphere. Earth and Space Science 6:411–432. https://doi.org/10.1029/2018EA000546
Lomidze L, Burchill JK, Knudsen DJ, Huba JD (2021) Estimation of ion temperature in the upper ionosphere along the Swarm satellite orbits. Earth Space Sci. https://doi.org/10.1029/2021EA001925
Merayo JÉMG, Jørgensen JL, Friis-Christensen E, Brauer P, Primdahl F, Jørgensen PS et al (2008) The swarm magnetometry package. In: Sandau R, Röser H-P, Valenzuela A (eds) Small satellites for Earth observation. Springer, Netherlands, pp 143–151. https://doi.org/10.1007/978-1-4020-6943-7_13
Mott-Smith HM, Langmuir I (1926) The theory of collectors in gaseous discharges. Phys Reviews 28(727):1926
Pakhotin IP, Mann IR, Lysak RL, Knudsen DJ, Gjerloev JW, Rae IJ et al (2018) Diagnosing the role of Alfvén waves in Magnetosphere-ionosphere coupling: swarm observations of large amplitude nonstationary magnetic perturbations during an interval of northward IMF. J Geophys Res Space Physics 123:326–340. https://doi.org/10.1002/2017JA024713
Pakhotin IP, Mann IR, Knudsen DJ, Lysak RL, Burchill JK (2020) Diagnosing the role of Alfvén waves in global field-aligned current system dynamics during southward IMF: swarm observations. J Geophys Res Space Phys. https://doi.org/10.1029/2019JA027277
Pakhotin IP, Mann IR, Xie K et al (2021) Northern preference for terrestrial electromagnetic energy input from space weather. Nat Commun 12:199. https://doi.org/10.1038/s41467-020-20450-3

Pakhotin and Burchill (2021) Swarm LP ion drift and effective mass product definition, swarm data, innovation, and science cluster (Technical Report). Report no.: SW-TN-UoC-GS-001: 1dA, 30 Aug 2021 (European Space Agency, 2021)
Park J, Lühr H, Stolle C, Rodriguez-Zuluaga J, Knudsen DJ, Burchill JK, Kwak Y-S (2016) Statistical survey of nighttime midlatitude magnetic fluctuations: their source location and Poynting flux as derived from the Swarm constellation. J Geophys Res Space Phys 121:11235–11248. https://doi.org/10.1002/2016JA023408
Resendiz Lira PA, Marchand R (2021) Simulation inference of plasma parameters from Langmuir probe measurements. Earth Space Sci. https://doi.org/10.1029/2020EA001344
Resendiz Lira PA, Marchand R, Burchill J, Förster M (2019) Determination of swarm front plate's effective cross section from kinetic simulations. IEEE Trans Plasma Sci 47(8):3667–3672
Rother M, Schlegel K, Lühr H (2007) CHAMP observation of intense kilometer-scale field aligned currents, evidence for an ionospheric Alfvén resonator. Ann Geophys 25(7):1603–1615. https://doi.org/10.5194/angeo-25-1603-2007
Smirnov A, Shprits Y, Zhelavskaya I, Lühr H, Xiong C, Goss A et al (2021) Intercalibration of the plasma density measurements in Earth's topside ionosphere. J Geophys Res Space Phys. https://doi.org/10.1029/2021JA029334
Truhlik V, Bilitza D, Třísková L (2015) Towards better description of solar activity variations in IRI ion composition model. Adv Space Res 55(8):2099–2105. https://doi.org/10.1016/j.asr.2014.07.033
Tu W, Xiang Z, Morley SK (2019) Modeling the magnetopause shadowing loss during the June 2015 dropout event. Geophys Res Lett 46:9388–9396. https://doi.org/10.1029/2019GL084419
Vasyliūnas VM (2012) The physical basis of ionospheric electrodynamics. Ann Geophys 30:357–369. https://doi.org/10.5194/angeo-30-357-2012
Verkhoglyadova OP, Meng X, Mannucci AJ, Mlynczak MG, Hunt LA, Lu G (2017) Ionosphere-thermosphere energy budgets for the ICME storms of March 2013 and 2015 estimated with GITM and observational proxies. Space Weather 15:1102–1124. https://doi.org/10.1002/2017SW001650
Verkhoglyadova OP, Meng X, Mannucci AJ, McGranaghan RM (2018) Semianalytical estimation of energy deposition in the ionosphere by monochromatic Alfvén waves. J Geophys Res Space Phys 123:5210–5222. https://doi.org/10.1029/2017JA025097
Weimer DR (2005) Improved ionospheric electrodynamic models and application to calculating Joule heating rates. J Geophys Res 110:A05306. https://doi.org/10.1029/2004JA010884
Woodman RF, Hoz La (1976) C. Radar observations of F region equatorial irregularities. J Geophys Res 81:5447–5466
Xiong C, Jiang H, Yan R, Lühr H, Stolle C, Yin F et al (2022) Solar flux influence on the in-situ plasma density at topside ionosphere measured by Swarm satellites. J Geophys Res Solid Earth. https://doi.org/10.1029/2022JA030275
Yamazaki Y, Maute A (2017) Sq and EEJ—a review on the daily variation of the geomagnetic field caused by ionospheric dynamo currents. Space Sci Rev 2017(206):299–405

Publisher's Note

Springer Nature remains neutral with regard to jurisdictional claims in published maps and institutional affiliations.

Submit your manuscript to a SpringerOpen journal and benefit from:

- ► Convenient online submission
- ► Rigorous peer review
- ► Open access: articles freely available online
- ► High visibility within the field
- ► Retaining the copyright to your article

Submit your next manuscript at ► springeropen.com